PERGAMON

Acta mater. Vol. 47, No. 12, pp. 3353–3366, 1999

Printed in Great Britain
PII: S1359-6454(99)00214-1
1359-6454/99 $20.00 + 0.00

PHASE FRACTION, TEXTURE AND STRAIN EVOLUTION IN SUPERELASTIC NiTi AND NiTi–TiC COMPOSITES INVESTIGATED BY NEUTRON DIFFRACTION

R. VAIDYANATHAN[1], M. A. M. BOURKE[2] and D. C. DUNAND[1]†

[1]Department of Materials Science and Engineering, Massachusetts Institute of Technology, Cambridge, MA 02139, U.S.A. and [2]LANSCE/MST, Los Alamos National Laboratory, Los Alamos, NM 87545, U.S.A.

(Received 17 March 1999; accepted 8 July 1999)

Abstract—Samples of superelastic NiTi and superelastic NiTi reinforced with 10 vol.% TiC particles were deformed under uniaxial compression to 975 MPa while neutron diffraction spectra were simultaneously collected. Despite the presence of stiff TiC particles, a macroscopic strain of 3% was obtained in the composite on loading and was fully recovered on unloading. The diffraction spectra were analyzed by Rietveld refinement that included a spherical harmonic description of the texture and a lattice plane (*hkl*) dependent formulation of the elastic strain. The experiments provided bulk, phase-specific measurements of the evolution of phase fractions, texture and strains during the reversible stress-induced austenite to martensite transformation responsible for the large recoverable strains. For the composite, Eshelby elastic theory is used to predict the discrete phase strains measured by neutron diffraction. The observed behavior suggests that the martensite accommodates the mismatch with the transforming austenite (while they co-exist) and the TiC particles (in the case of the composite). © *1999 Acta Metallurgica Inc. Published by Elsevier Science Ltd. All rights reserved.*

Keywords: Composites; Neutron scattering; Phase transformations; Shape memory; Superelasticity

1. INTRODUCTION

The intermetallic NiTi with near-equiatomic composition can exhibit a reversible, thermoelastic transformation between a cubic (B2), parent austenite phase and a monoclinic (B19′), martensite phase near room temperature. While slip by dislocation occurs in these alloys at higher applied stresses, alternative deformation mechanisms can dominate at lower stresses and result in superelasticity or the shape-memory effect. Austenitic NiTi alloys can demonstrate superelastic behavior wherein on mechanical loading, tensile strains as high as 8% may result from the formation of stress-induced martensite. On unloading, the martensite becomes unstable and reverts to austenite with concomitant recovery of all the accumulated macroscopic strain. In martensitic NiTi, twinning is the dominant mechanism of deformation and thermal recovery of twinned martensite is associated with the shape-memory effect [1, 2].

Extensive knowledge exists concerning the deformation of metal matrix composite systems with stiff ceramic reinforcing phases (such as Al–SiC) where the matrix deforms by slip after initial elastic deformation [3]. However, little is known about composites with matrices exhibiting alternative deformation mechanisms (e.g. twinning or stress-induced transformations). The thermoelastic phase transformation and/or twinning deformation in NiTi can be expected to be affected by the presence of stiff ceramic particles which not only produce residual internal stresses (due to thermal mismatch) but also partition externally applied stresses. Consequently, the mechanical deformation behavior of such composites is both of theoretical interest (to better understand such deformation mechanisms) and practical interest (as superelastic composites).

Dunand and co-workers have carried out investigations to systematically characterize such NiTi-based shape-memory composites (martensitic NiTi matrix reinforced with TiC). The thermal transformation behavior [4, 5], the bulk mechanical properties in compression [6], the subsequent shape-memory recovery [7] and the study by neutron diffraction of twinning deformation and shape-memory recovery [8, 9] have been investigated. Key results from these investigations are summarized in Ref. [10]. To the best of our knowledge, there has been no study providing information on the mechanical behavior of an austenitic NiTi matrix with a reinforcing ceramic phase where the matrix is

†To whom all correspondence should be addressed. Present address: Department of Materials Science and Engineering, Northwestern University, Evanston, IL 60208, U.S.A.

capable of deforming by reversibly forming stress-induced martensite from austenite.

While both neutron and X-ray diffraction can provide phase specific information on the evolving texture, phase fractions and discrete phase strains during a stress-induced transformation, the penetration depth of neutrons is typically several millimeters compared to a few micrometers for a conventional X-ray source. Thus using a neutron source, free surface stress effects become negligible and diffraction measurements are representative of the bulk behavior. We demonstrated in an earlier publication [11] the ability to observe stress-induced austenite to martensite transformations in NiTi by obtaining neutron diffraction data while NiTi was subjected to loading. We extended this investigation to the fabrication and testing of superelastic NiTi reinforced with 10 and 20 vol.% TiC particles [12]. However, in that work, due to limitations in loading we were restricted to low volume fractions of martensite and did not obtain a complete austenite to martensite transformation. In the present paper, we further investigate the behavior of unreinforced NiTi and particle reinforced NiTi by carrying out neutron diffraction measurements during compression loading and unloading. To understand the mechanical behavior of the composites, we also investigate the individual austenite and martensite phases as they co-exist and evolve with stress in the monolithic NiTi.

2. EXPERIMENTAL PROCEDURES

2.1. Sample fabrication

Pre-alloyed NiTi powders (99.9% pure, 49.4 at.% Ni, size between 44 and 177 μm, from Special Metals Corp., NY) were blended with Ni powders (99.9% pure, size between 44 and 177 μm, from Special Metals Corp., NY) and TiC powders (99.9% pure, 44 μm average size, from Atlantic Equipment Engineers, NJ). The powders were packed in a cylindrical low carbon steel container (thickness 0.318 cm, internal diameter 2.5 cm, length 12 cm, lined with a boron nitride coated nickel foil to prevent carbon contamination) and were subjected to Hot Isostatic Pressing (HIP) at 1065°C and 100 MPa for 3 h. The consolidated billets had the following nominal compositions:

(a) unreinforced NiTi (51.0 at.% Ni);
(b) 10 vol.% TiC in a NiTi (51.0 at.% Ni) matrix.

The billets were electro-discharge-machined into cylindrical specimens 10 mm in diameter and 24 mm in length. These monolithic and composite samples, designated as NiTi (S1) and NiTi–TiC (S1), respectively, were solutionized at 1000°C for 1 h and oil-quenched to room temperature in titanium-gettered flowing argon, annealed at 400°C for 1 h in air and quenched in ice-water.

The samples were first tested to 625 MPa under uniaxial compression as outlined in the following section, before being reduced in dimensions by electro-discharge-machining to cylindrical samples 8 mm in diameter and 20 mm in length. This was done to apply larger stresses given the limited capacity of the loading frame. By using the same samples, it was hoped that uncertainties associated with the introduction of a new sample would be avoided. The heat treatment described previously was again followed. The resulting reduced gauge samples, designated as NiTi (S2) and NiTi–TiC (S2), respectively, were again tested as described below.

2.2. Neutron diffraction and mechanical testing

Information on the experimental set-up can be found elsewhere [9, 13, 14] and is only summarized here. Neutron diffraction measurements were performed in "time of flight" mode using the Neutron Powder Diffractometer (NPD) at the pulsed neutron source at Los Alamos National Laboratory (LANL). The samples were loaded in compression while neutron diffraction spectra were simultaneously acquired in three scattering geometries. The loading axis formed an angle of 45° with the incident neutron beam, allowing measurements for which the scattering vector was parallel and perpendicular to the loading axis. Since the incident beam is polychromatic, by choosing data from the appropriate detectors, information from crystallographic planes parallel or perpendicular to the loading direction can be obtained as shown in Fig. 1. A third detector was used in back-scattering geometry. An extensometer was attached to the samples to record macroscopic strain during the experiments.

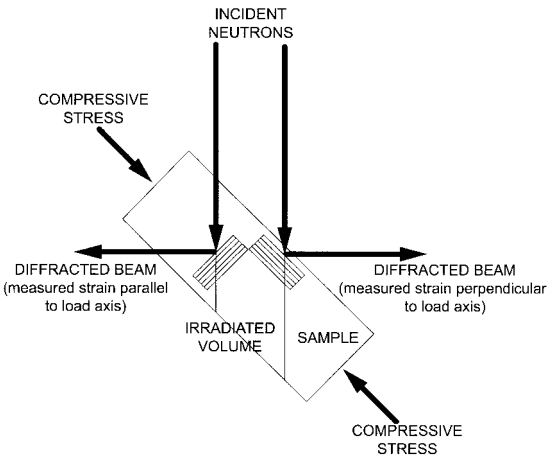

Fig. 1. Schematic of experimental set-up at Los Alamos National Laboratory showing the incident beam and two of the three diffracted beams with respect to the loading direction. The irradiated volume is about 1 cm^3.

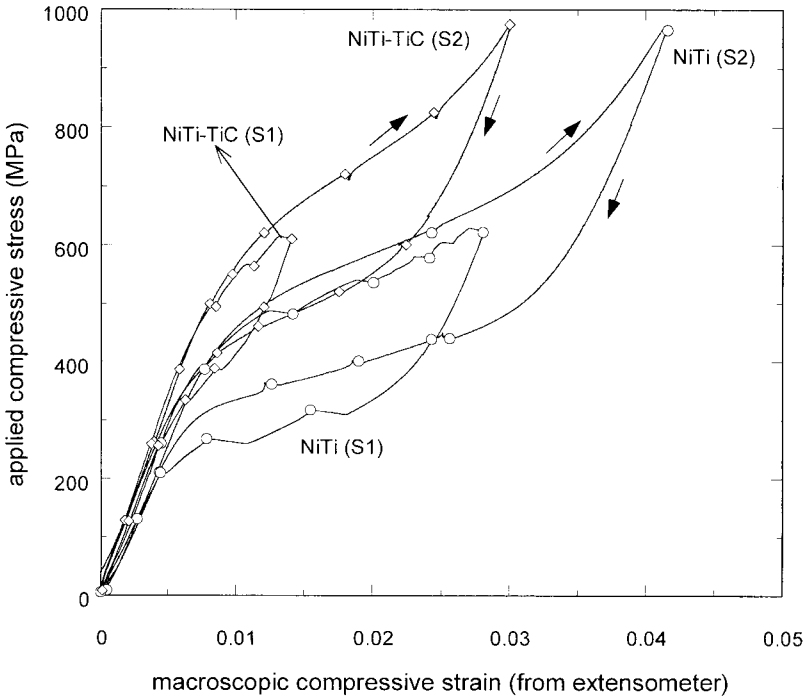

Fig. 2. Applied compressive stress vs macroscopic compressive strain measured by extensometry for NiTi and NiTi–TiC. The symbols indicate the stresses at which neutron diffraction spectra were obtained.

Results from four tests at room temperature corresponding to NiTi and NiTi–TiC are presented. The larger samples (S1) were tested to 625 MPa under uniaxial compression (stroke control at 3 mm/min) while neutron diffraction data were simultaneously obtained. For simplicity, compressive stresses and strains are reported as positive numbers in this paper. Prior to making the measurements in the beam, the samples were "trained" by loading twice to 625 MPa (load–unload cycle) at a stroke speed of 3 mm/min. The purpose of these mechanical training cycles was to homogenize and remove any initial instabilities associated with the transformation [15]. A non-recoverable compressive plastic strain of 0.1% was recorded after the first training cycle but none was noted after the second or the diffraction cycle. The data obtained with the S1 samples were the same as those obtained in our previous work [12].

The smaller samples (S2), owing to their reduced diameter, were tested to 975 MPa under uniaxial compression (stroke control at 0.1 mm/min) with simultaneous neutron diffraction. These cycles were also obtained after the same training procedure as the larger samples. Diffraction data were obtained by interrupting the loading and unloading parts of the cycle at the stresses shown in Fig. 2.

2.3. Sample characterization

Within the resolution of optical microscopy [16], the samples were observed to be pore-free with unreacted interfaces in the composites. In addition, a uniform distribution of equiaxed TiC particles was observed in NiTi–TiC. The average grain size was determined by image analysis to be 20 μm with no statistically significant differences between the monolithic and composite samples. Density measurements by water displacement showed that NiTi and NiTi–TiC were 99.8 and 99.7%, respectively, of their theoretical density.

Differential scanning calorimetry with a Perkin Elmer DSC-7 Calorimeter at a rate of 1 K/min under nitrogen cover gas was used in an attempt to determine the martensite start (M_s) and martensite finish (M_f) temperatures for the two compositions. Temperatures as low as −140°C were approached with no observable transformation. Furthermore, a neutron diffraction spectrum recorded for a NiTi specimen cooled to −253°C with liquid helium confirmed that the structure remained B2 austenitic.

3. NEUTRON DIFFRACTION DATA ANALYSIS

In the case of a reversible austenite to martensite transformation, grains of austenite do not transform randomly [11]. Rather, the austenite develops texture because of the preferential transformation to martensite of grains favorably oriented with respect to the stress and able to accommodate the transformation strain. Correspondingly, the diffracted intensity of some austenite peaks diminishes

more rapidly than others, resulting in single peak (*hkl*) reflections not being representative of the overall transformation. In addition, single peak reflections include anisotropic contributions from crystal geometry and strain redistribution especially arising due to the transformation. In a companion article [17], these issues have been discussed and a methodology established to analyze diffraction spectra in the case of such transformations. Here the outcome of that work is summarized with the emphasis placed on obtaining phase fraction, texture and strain information to help explain the mechanical responses of NiTi and NiTi–TiC.

By using the Rietveld refinement [18] technique implemented in the LANL code GSAS [19], the information used incorporates the entire diffraction spectrum. In the Rietveld method, a mathematical model is developed that calculates an intensity, Y_c, at every point in the spectrum, i.e.

$$Y_c = Y_b + \sum_h SKF_h^2 P(\Delta T_h) \tag{1}$$

where the first term, Y_b, is the background intensity and the second term is the Bragg scattering containing a scale factor, S, a correction factor, K, a structure factor, F_h and a profile function, $P(\Delta T_h)$, as determined by the displacement, ΔT_h, of the profile point from the reflection position. Within the correction factor, K, is a term which describes the change in Bragg intensity for a reflection due to texture. A generalized spherical harmonic description [20, 21] is used to account for the evolving texture in the austenite and martensite phases. The refinement procedure varies selected parameters including phase volume fractions, atom positions and texture until the calculated spectrum matches the measured spectrum in a least squares fit. Errors are quantified and are associated with the statistics of such a fit. The profile function which fitted the data best is a combination of two functions—one is the result of convoluting two back-to-back exponentials with a Gaussian and the other is a linear combination of a Lorentzian and a Gaussian (pseudo-Voigt).

For the austenite and TiC phases, two formulations of the strain are used. In the first approach, the refinement procedure determines a lattice parameter by fitting many individual reflections. The elastic lattice strain is then reported as

$$\varepsilon_{\text{aus}} = \frac{a_s^{\text{aus}} - a_0^{\text{aus}}}{a_0^{\text{aus}}}$$

$$\varepsilon_{\text{TiC}} = \frac{a_s^{\text{TiC}} - a_0^{\text{TiC}}}{a_0^{\text{TiC}}} \tag{2}$$

where a_s are the austenite or TiC lattice parameters under an applied compressive stress and a_0 are the respective lattice parameters under no external load. A compressive stress of 8 MPa was used to hold the sample horizontally in the stress rig and corresponds to this "no load" condition. In equation (2), no attempt was made to accommodate the lattice plane (*hkl*) specific anisotropy and the implicit assumption is made that either the strain has no lattice plane dependence or is a reasonable average over all lattice planes. This formulation has been demonstrated to empirically capture the "isotropic" phase strain despite anisotropy in cubic Fe [22], hexagonal Be [23] and in austenite in NiTi [17].

In the second approach, a strain anisotropy term is incorporated in the Rietveld procedure and the strain is reported for a specific plane as a contribution of isotropic (*hkl*-independent) and anisotropic (*hkl*-dependent) components:

$$\varepsilon_{\text{aus}}^{hkl} = \varepsilon_{\text{aus}}^{\text{iso}} - A_{hkl}\varepsilon_{\text{aus}}^{\text{aniso}}$$

$$\varepsilon_{\text{TiC}}^{hkl} = \varepsilon_{\text{TiC}}^{\text{iso}} - A_{hkl}\varepsilon_{\text{TiC}}^{\text{aniso}} \tag{3}$$

where A_{hkl} is $(h^2k^2 + h^2l^2 + k^2l^2)/(h^2 + k^2 + l^2)^2$. The isotropic strain component, ε^{iso}, is determined by shifting individual lattice reflections so as to account for a change in the lattice parameter, as in equation (2). The anisotropic strain component, $\varepsilon^{\text{aniso}}$, further shifts individual reflections proportional to A_{hkl}. The A_{hkl} dependence is introduced because in a cubic single crystal the plane specific modulus, E_{hkl}, can be expressed as

$$\frac{1}{E_{hkl}} = S_{11} - 2\left(S_{11} - S_{12} - \frac{S_{44}}{2}\right)A_{hkl} \tag{4}$$

where S_{ij} is the single crystal compliance tensor in collapsed matrix notation [24]. The A_{hkl} dependence was originally formulated to capture the elastic anisotropy in single crystals and has been used here since it *empirically* captures the elastic anisotropy in polycrystals [22] and the anisotropy introduced by the austenite to martensite transformation in polycrystalline NiTi [17].

Martensitic diffraction peaks were not characterized for strain development since the lattice parameter value for the nascent martensite cannot be easily determined. In addition, the large number of broad overlapping reflections due to the low symmetry and scale of the monoclinic martensite make it difficult for the Rietveld refinement to converge while strains are fitted in the martensite. For the martensite, the emphasis was on accurately modeling its volume fraction and texture.

4. RESULTS

Owing to the difficulty in machining the composites and the large sample volume requirements, compression rather than tension tests were performed. While differences in tension and compression exist for NiTi [25], they are expected to be limited to the magnitude of the observed behavior (e.g. recoverable strain) rather than differences in

Table 1. Young's moduli (GPa) for NiTi and NiTi–TiC measured by extensometry

Sample	Young's modulus (GPa)
NiTi (S1)	50 ± 2
NiTi (S2)	51 ± 2
NiTi–TiC (S1)	58 ± 2
NiTi–TiC (S2)	59 ± 2

mechanisms. Figure 2 shows the stress–strain response of the four samples. The pronounced steps in the first set of measurements, i.e. in the larger diameter NiTi (S1) and NiTi–TiC (S1) can be attributed to the higher loading rate and the consequent temperature effects [26–28]. The differences in the stress–strain envelopes of the S1 and S2 samples of the same material in Fig. 2 can be attributed to a small difference in the ambient temperature (less than 5°C), probably due to a different level of air cooling of the hydraulic equipment in the enclosed testing volume. Both these issues are discussed in Ref. [17]. Despite the difference in testing temperatures, data from the S1 and S2 samples can be combined if the superelastic strain is reported. Superelastic strain refers to the macroscopic strain (measured by extensometry) from which the elastic contribution was subtracted. Since the transformation is thermoelastic, the superelastic strain is representative of the transformation, independent of temperature.

Table 1 lists the Young's moduli of NiTi and NiTi–TiC obtained from a fit to the initial linear portion of the macroscopic stress–strain curve (before the onset and after the completion of the transformation on loading and unloading, respectively). As expected, no significant differences exist between samples S1 and S2 of the same material. Figure 3 contrasts typical spectra corresponding to NiTi and NiTi–TiC at 975 MPa and at the no load condition. A qualitative examination of the peak intensities at 975 MPa shows that there is more martensite in NiTi than in NiTi–TiC. By using data from all three sets of detectors with a generalized spherical harmonic texture formulation in the Rietveld refinement, the amount of martensite present is quantified at the various stresses. A typical refinement is shown in Fig. 4. The volume fraction of martensite is presented as a function of the superelastic strain in Fig. 5 for all four samples and data obtained during the loading part of the cycle are distinguished from those obtained during the unloading part. Elastic moduli of 51 GPa for NiTi and 59 GPa for NiTi–TiC from Table 1 were used to determine the superelastic strain by subtracting

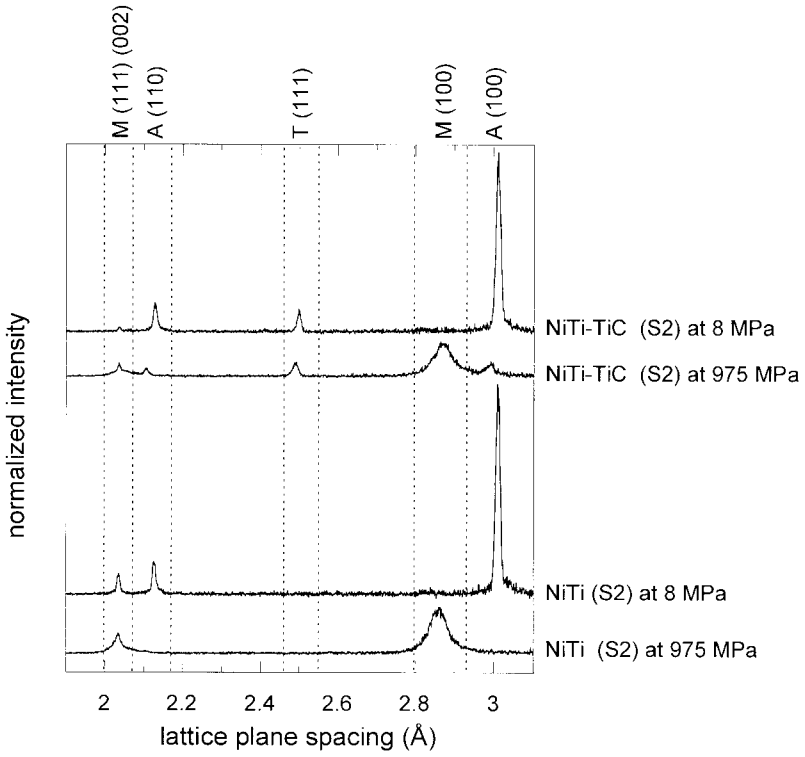

Fig. 3. Section of normalized neutron diffraction spectra from NiTi and NiTi–TiC under at 8 and 975 MPa with austenite (A), martensite (M) and TiC (T) peaks identified. The spectra shown here are from diffracting lattice planes perpendicular to the loading axis. Diffraction from steel in the extensometer knife edges contaminates the M(111) reflection position. This did not compromise the refinement.

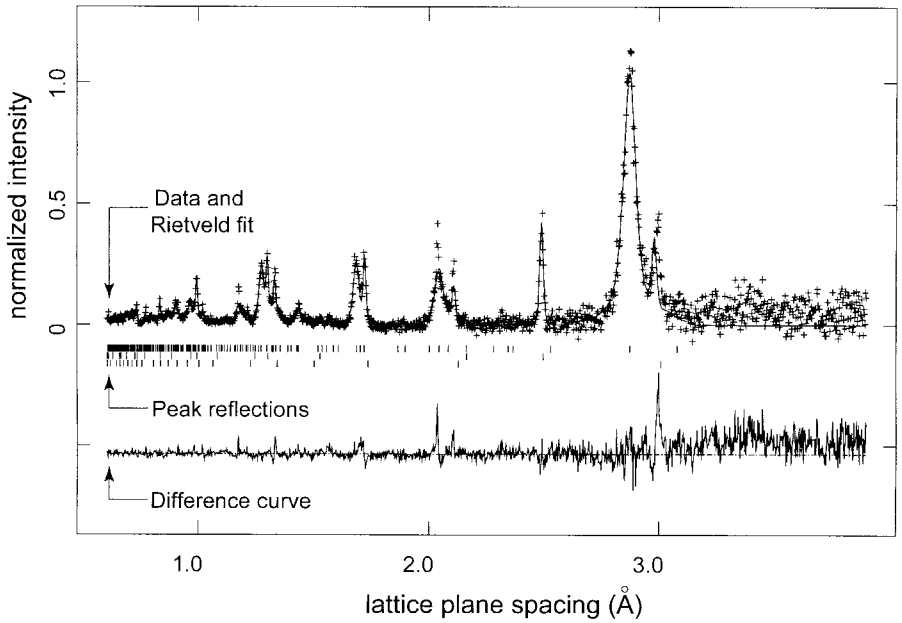

Fig. 4. A typical GSAS Rietveld refinement output [shown here for NiTi–TiC (S2) at 975 MPa] for diffracting lattice planes perpendicular to the loading axis. The crosses are the measured data; the line through them is the Rietveld least squares fit. The tick marks indicate reflections from the martensite, austenite and TiC phases (from top to bottom). The difference curve between refinement and measurement is also shown at the bottom of the figure.

the elastic contribution from the macroscopic strain. The volume fraction of martensite in NiTi–TiC is expressed as a fraction of the transformable matrix and the superelastic strain is divided by 0.9 since only 90% of the sample can generate recoverable strain. The validity of the refinement is supported by the predicted TiC volume fractions (not input parameters during the Rietveld procedure) which were within 0.8 vol.% of the nominal volume fraction (10 vol.%).

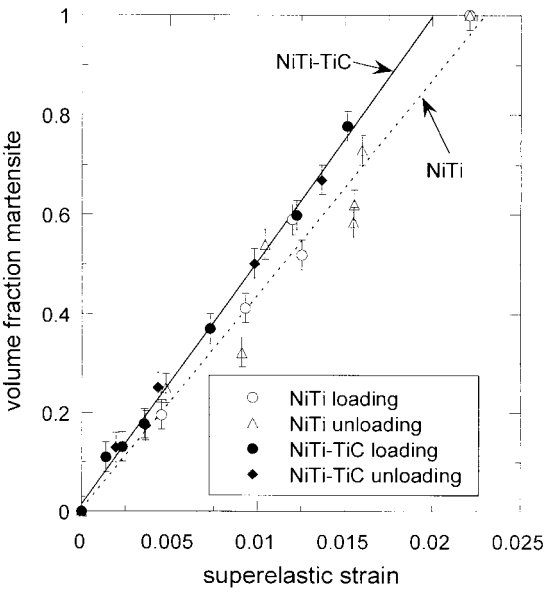

Fig. 5. Volume fraction of martensite obtained by Rietveld refinement as a function of the superelastic strain in NiTi and NiTi–TiC (samples S1 and S2).

The sharpness of the texture can be characterized by a single parameter, the texture index J [29]:

$$J = \oint [f(g)]^2 \, \mathrm{d}g \tag{5}$$

where $f(g)$ is the orientation distribution function which maps the probability of each of the possible grain orientations, g, with respect to the external sample dimensions and the integration is over all orientation space. Using a series expansion and given the orthogonality of generalized spherical harmonics, it can be shown [20] that J varies between unity and infinity (corresponding to random orientation and to ideal single crystals, respectively). Typical values of the texture index are: 2–5 for moderate texture (e.g. 70% rolled steel has an index of 3–4), 10–15 for a strong texture (e.g. wire drawing) [30]. Figure 6 shows the martensite texture index for all four samples in NiTi and NiTi–TiC. The texture index was determined to be inadequate to track the smaller changes in texture in the austenite phase.

The texture index merely indicates trends in texture evolution, whereas the actual distribution is obtained from axial distribution plots. These plots are used here because of the cylindrical symmetry in the samples and correspond to a radial slice of the pole figure. In an axial distribution plot, the y-axis is a measure of the number of grains that are oriented at an angle ϕ between the normal to the chosen plane and the loading axis (in this case),

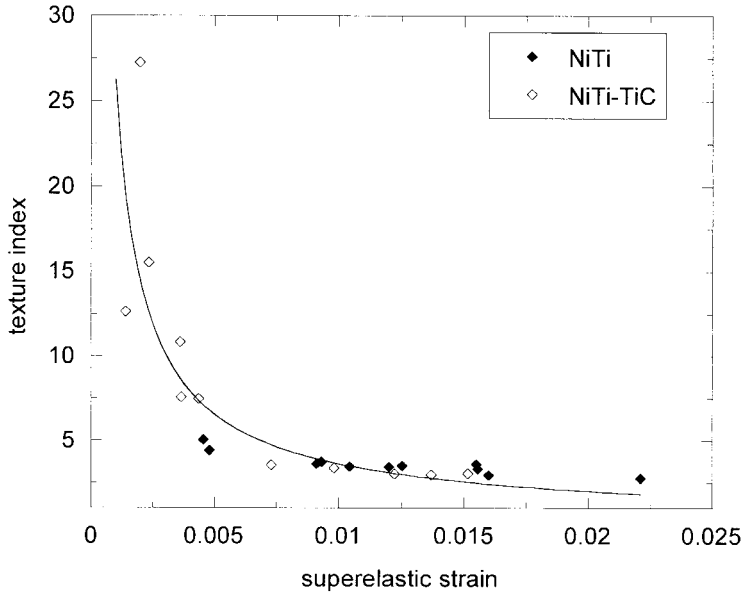

Fig. 6. Martensite texture index in NiTi and NiTi–TiC (samples S1 and S2) as a function of superelastic strain. The line is a power law fit without physical significance.

compared to a randomly oriented polycrystal. Thus a random polycrystalline sample would be represented by a horizontal line at unity. There is no physical significance associated with values of less than zero, which in these plots is an outcome of the global normalization procedure. Figure 7 shows (100) axial distribution plots for austenite in NiTi (S1) under no load (after training) and with increasing stress to 625 MPa. Figures 8 and 9 are axial distribution plots that compare martensite that is formed in the presence and absence of TiC particles, respectively, at the same superelastic strain. Two superelastic strains are considered, i.e. 0.004 and 0.012 and the orientations of (100) planes are plotted in these figures. Only representative axial distribution plots are presented here but identical behavior was observed in other spectra.

Figure 10 shows elastic lattice strains obtained from Rietveld analysis [equation (2)] in the austenite in NiTi for samples S1 and S2 during loading and unloading. Figure 11 similarly shows elastic lattice strains obtained from Rietveld analysis [equation (2)] for both samples in the austenite and TiC phases of NiTi–TiC. The individual elastic

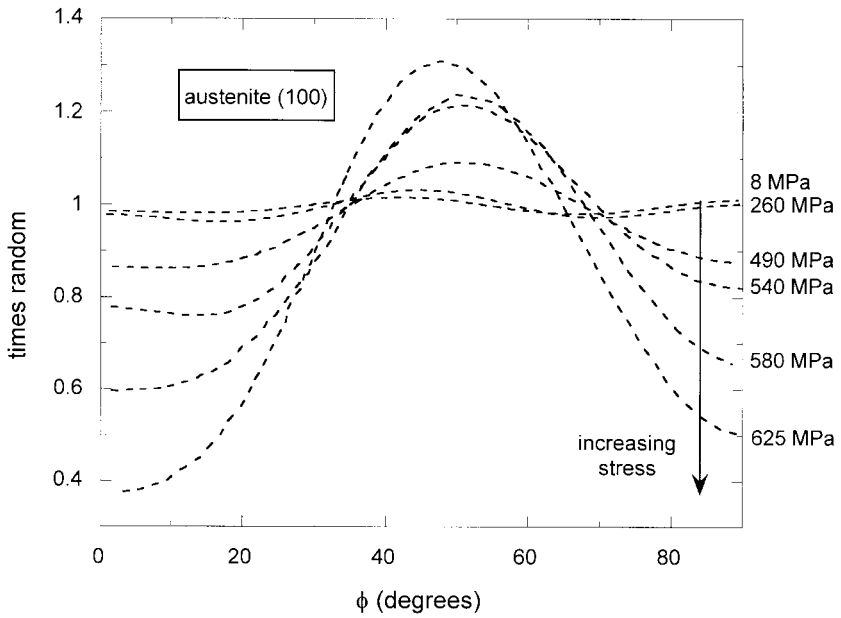

Fig. 7. (100) axial distribution plots for austenite in NiTi (S1) with increasing applied stresses. ϕ is the angle between the (100) plane normal and the loading axis.

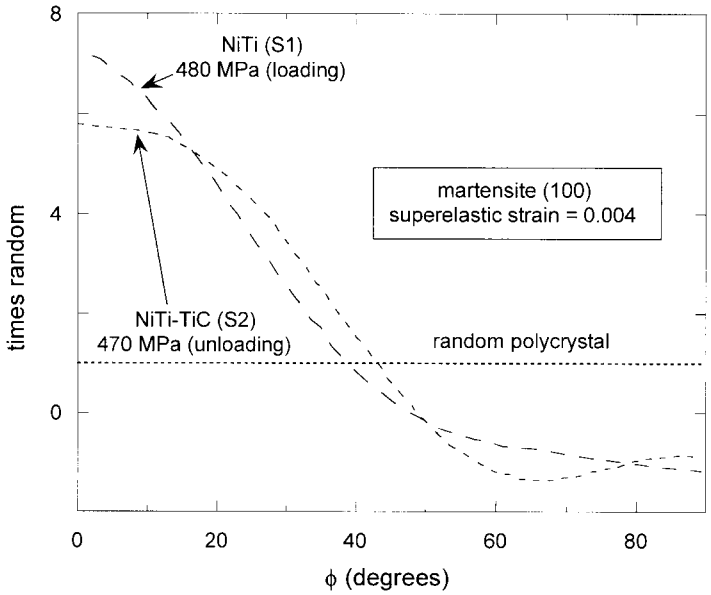

Fig. 8. (100) axial distribution plots for martensite in NiTi and NiTi–TiC at a superelastic strain of 0.004. ϕ is the angle between the (100) plane normal and the loading axis.

phase strains as predicted from Eshelby theory are also shown in Fig. 11. The reported strains from neutron diffraction measurements are off-set so as to coincide (in the no load condition) to the residual coefficient of thermal mismatch stresses predicted from Eshelby theory. The errors in Figs 10 and 11 are about the size of the markers, i.e. $\pm$half marker width. For NiTi–TiC (S1), the average isotropic strain in austenite [ε_{aus} in equation (2)] is plotted against its anisotropic component [$\varepsilon_{aus}^{aniso}$ in equation (3)] during loading and unloading in Fig. 13. The motivation for presenting this plot is to associate the behavior of the anisotropic component of the strain with the onset and completion of the transformation. Identical trends in the anisotropic component of strain were observed in both samples of NiTi–TiC.

5. DISCUSSION

The NiTi–TiC system is chemically inert over a large range of compositions [31, 32]. This observation has also been confirmed by microprobe analysis in the case of martensitic NiTi reinforced with TiC [4]. The unreacted interfaces observed in our tested samples further suggest that the TiC par-

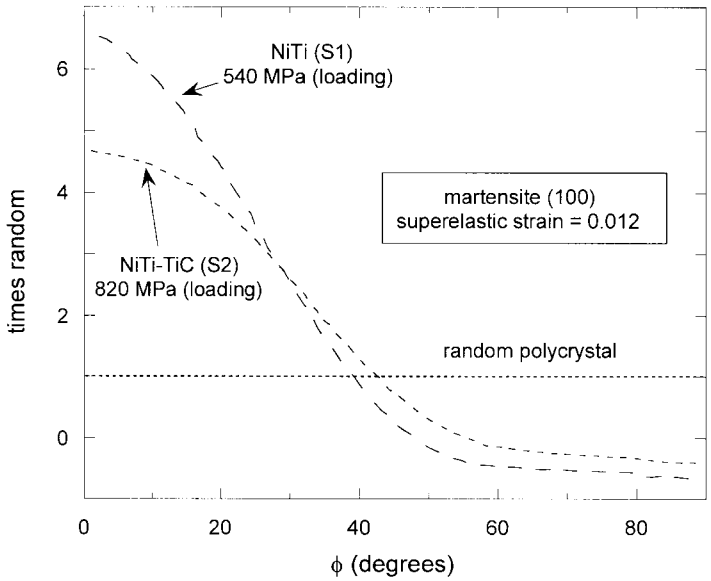

Fig. 9. (100) axial distribution plots for martensite in NiTi and NiTi–TiC at a superelastic strain of 0.012. ϕ is the angle between the (100) plane normal and the loading axis.

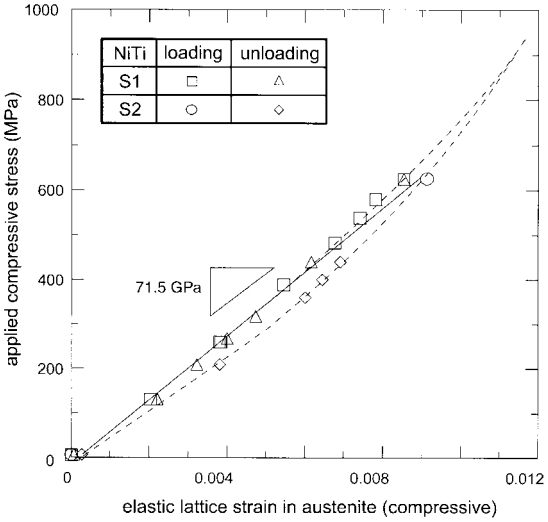

Fig. 10. Elastic lattice strain obtained from Rietveld analysis [equation (2)] in the austenite phase in NiTi (samples S1 and S2) during loading and unloading, as a function of applied stress. The best fit line through all the data is also shown. The dashed curve illustrates qualitatively a non-linear response at higher stress that includes (a) the hysteresis in the transformation and (b) austenite transferring load to the martensite.

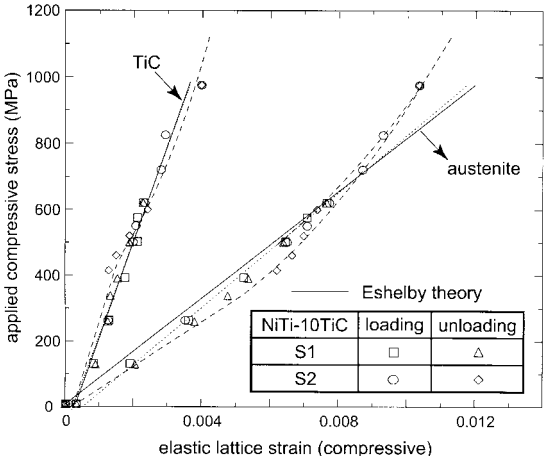

Fig. 11. Elastic lattice strains obtained from Rietveld analysis [equation (2)] in the austenite and TiC phases in NiTi–TiC (samples S1 and S2) during loading and unloading, as a function of applied stress. Phase strains predicted by Eshelby elastic theory are also shown by the bold line. The best fit line through the data corresponding to each phase is the dotted line. The dashed curve illustrates qualitatively a non-linear response at higher stress that includes (a) the hysteresis in the transformation and (b) load transfer in austenite and TiC.

ticles, which were almost perfectly stoichiometric with a composition of 49.8 ± 0.1 at.% C (as determined by combustion analysis with infra-red detection), behave as a chemically inert reinforcement. From Ref. [33], the temperature at which martensite should start to form (M_s) when austenitic NiTi (51.0 at.% Ni) is cooled is expected to be around -50°C. However, this is inconsistent with our experience of austenite not transforming to martensite even at -253°C despite having a nominal composition of 51.0 at.%. One possible explanation is that some oxygen that was present on the surface of the original powder prior to HIP forms $Ti_4Ni_2O_x$ (as observed experimentally in similar samples in Ref. [34]). This will deplete the Ti content of NiTi and consequently depress the M_s temperature, explaining why the transformation could not be thermally induced. Nevertheless, given the equivalence of stress and temperature in such transformations, the ease of transformation to martensite by stress is puzzling. Despite the preceding ambiguity, the comparable densities (the small difference is attributed to porosity in TiC), grain sizes and the lack of interfacial reaction between NiTi and TiC lead us to believe that the mechanical behavior of NiTi and NiTi–TiC can be directly compared in this work.

5.1. Macroscopic mechanical response of NiTi and NiTi–TiC

In addition to the differences in elastic moduli (Table 1), the following observations in the monolithic and composite material can be made from Fig. 2.

(a) The applied stress at which austenite transforms to martensite (on loading) and transforms back to austenite (on unloading) is higher in the composite.

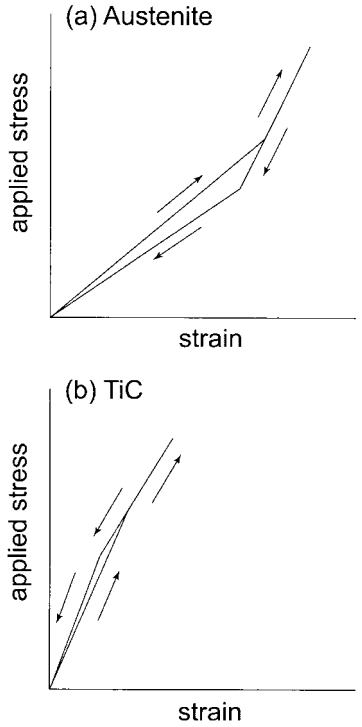

Fig. 12. (a) Schematic of an applied stress vs elastic strain response that includes the hysteresis in the transformation and load transfer from austenite. (b) Corresponding schematic showing load being transferred to TiC. For simplicity, straight lines are used to represent the evolving strains.

Table 2. Polycrystalline elastic constants determined from single crystal data for austenite from three averaging methods, i.e. (1) Hashin–Shtrikman lower bound, (2) Hashin–Shtrikman upper bound [38], and (3) Hill [41]

Averaging method	For $c_{11} = 137$ GPa, $c_{12} = 101$ GPa, $c_{44} = 35$ GPa [36] Young's modulus (GPa)	Shear modulus (GPa)	Poisson's ratio	For $c_{11} = 162$ GPa, $c_{12} = 129$ GPa, $c_{44} = 35$ GPa [37] Young's modulus (GPa)	Shear modulus (GPa)	Poisson's ratio
1	74.4	26.8	0.39	72.9	25.8	0.41
2	75.4	27.2	0.39	74.3	26.3	0.41
3	74.5	26.8	0.39	73.0	25.8	0.41

(b) The stress–strain gradient during the transformation is steeper in the composite.

(c) The recoverable macroscopic strain is lower in the composite.

(d) The width of the stress–strain hysteresis (difference between the stresses corresponding to the onset and completion of the transformation) is larger in the composite.

A thermoelastic martensitic transformation is based on a balance of chemical free energy, elastic strain energy and interfacial energy during the course of the forward and reverse transformations [33]. The transformational shape change is accommodated elastically in the system and the build-up of this strain energy hinders further growth of martensite [35]. Thus thermodynamically, the additional elastic strain energy introduced by the interaction of martensite with the TiC particles would result in a steeper stress–strain gradient with increasing volume fraction of TiC. This increase in elastic strain energy would also imply that higher stresses will be needed to transform austenite to martensite with increasing volume fraction of TiC. The increase in the width of the stress–strain hysteresis may also be due to an increase in the frictional resistance to interface motion because of the TiC particles. In addition, load partitioning due to the stiffer TiC (i.e. the matrix stress being lower than the applied stress) will also contribute to these changes in critical stresses and stress–strain gradients. These two effects have not been decoupled in this work.

Starting from stiffness tensor values for austenite reported by Refs [36, 37], the elastic behavior of a polycrystal is determined as a single crystal average using the Hashin–Shtrikman [38] upper and lower bounds for elastic moduli of cubic polycrystals. The Voigt [39] and Reuss average [40] suggested by Hill [41] is also used and the results are tabulated in Table 2.

The matrix mean internal stress is determined using the Eshelby method [3, 9] as a result of thermal mismatch stresses upon cooling from the annealing temperature. For austenite, an elastic modulus of 74.5 GPa, a shear modulus of 26.8 GPa and a Poisson's ration of 0.39 are used as obtained in Table 2. For TiC, the room-temperature elastic constants measured in Ref. [42], i.e. $c_{11} = 515$ GPa, $c_{12} = 106$ GPa and $c_{44} = 179$ GPa are used. The equiaxed inclusions are assumed to be spherical for

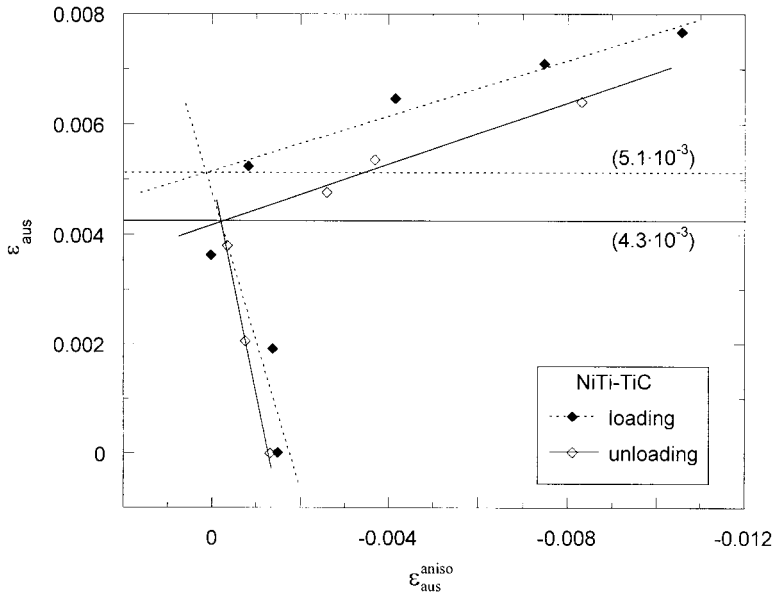

Fig. 13. Isotropic strain in austenite [ε_{aus} in equation (2)] plotted against its anisotropic component [$\varepsilon_{aus}^{aniso}$ in equation (3)] during loading and unloading in NiTi–TiC (S1). The strains at which changes in slope are observed are also shown.

this analysis. Using 11×10^{-6}/K as the average coefficient of thermal expansion for austenite and 7.3×10^{-6}/K as the average coefficient of thermal expansion of TiC [43, 44] and assuming, as observed experimentally [45, 46], that diffusion and creep processes relax the thermal mismatch stresses at temperatures above $0.65T_M$ (where T_M is the melting point, 1163°C for NiTi [43]), the matrix thermal expansion mismatch mean tensile stress is determined to be 25 MPa in NiTi–TiC.

The Eshelby method is also used to determine an average elastic modulus for the composite before the onset (and after the completion) of the transformation, i.e. when only austenite and TiC are present. A Young's modulus of 87.3 GPa is predicted, neglecting the small (i.e. 25 MPa) coefficient of thermal expansion mismatch stresses between the austenite matrix and TiC.

Thus there are significant discrepancies between the moduli obtained from extensometer measurements for both NiTi and NiTi–TiC (Table 1) and the theoretical predictions (Table 2 and Eshelby theory). There was no indication of texture in the austenite at these low stresses which could have possibly explained the differences in moduli (see Section 5.3). However, a likely explanation is that the extensometer measured non-elastic contributions (i.e. stress-induced transformation) even in the lower initial portion of the stress–strain curve. Assuming that favorable orientations of austenite transform to martensite at these low stresses (e.g. producing a compressive strain of 5.2% in the ⟨011⟩ direction with reference to the parent phase vector basis [47]), a mere 1 vol.% of martensite is needed every 78 MPa to explain the difference between the measured and predicted elastic modulus for NiTi. This small volume fraction of martensite is below the experimental sensitivity of neutron diffraction.

5.2. Phase fraction evolution

In Fig. 5 for both NiTi and NiTi–TiC, a linear relationship is observed during loading–unloading between the volume fraction of martensite formed and the superelastic strain. No hysteresis is observed between loading and unloading, confirming that the hysteresis observed in Fig. 2 is with respect to stress and not strain [48].

A relevant question that arises is whether the nascent martensite formed under stress can deform further to generate more recoverable strain. This is possible if the martensite is not in the optimal orientation with respect to the applied stress and growth/coalescence or reorientation by twinning of certain variants can produce more strain. To answer this question, NiTi and NiTi–TiC were further tested to higher stresses [16]. Fully transformed martensite begins to yield due to slip and some residual strain exists after unloading. Specifically, there was no evidence of the stress-induced martensite producing additional recoverable strain.

Figure 5 shows that a somewhat larger volume fraction of martensite is needed to generate the same superelastic strain when TiC particles are present. This indicates that the average transformation strains associated with martensite formation are smaller when TiC particles are present. This is understandable given that the most favorable variant, in terms of the macroscopic strain, may not be compatible with a non-transforming TiC particle in its proximity and may thus not form.

5.3. Texture evolution

The austenite is randomly oriented in the unloaded condition and remains so at least till 260 MPa, as seen by the two nearly horizontal lines in the axial distribution plots (Fig. 7). Consistent with our discussion [17], the remaining austenite exhibits increasing texture with increasing stress as martensite is formed because of its preferential transformation. In Fig. 7, from scattering geometry this corresponds to the preferential transformation of grains having their (100) lattice planes perpendicular and parallel to the loading axis. The martensite that forms under stress is also textured because of the nature of the transformation [33] and this explains its high texture indices in Fig. 6. From Fig. 6 it is also seen that for both NiTi and NiTi–TiC, martensite that exists at lower strains is more textured than that which exists at higher strains. Given the linear relationship in Fig. 5 and the decreasing texture in Fig. 6, a non-unique association between variant orientation and transformation strain is expected. This means that more than one orientation among the 24 variants should generate close to the same strain, because the martensite that forms at lower stresses generates the same strain as martensite that forms at higher stresses. This non-singular correspondence between variant orientation and strain has been previously outlined in Ref. [47].

From the texture index alone (Fig. 6), it is not clear whether TiC influences the texture of the stress-induced martensite. However, in the axial distribution plots (Figs 8 and 9), comparing the texture of martensite formed in the presence and absence of TiC at the same superelastic strain suggests that martensite in the presence of TiC is less textured. This is understandable since there are more spatial constraints for the formation of martensite when TiC is present. This situation is analogous to martensite forming at lower strains (where fewer constraints exist) being more textured than the martensite forming at higher stresses (where other martensite plates preclude certain orientations).

The preceding discussion on the evolution of phase fractions and texture is qualitatively consistent with the lower recoverable strain observed in the composite. The quantitative extension from texture and phase fractions to recoverable strain in

polycrystals is not straightforward because of the difficulty in relating the large number of variant orientations in the various grains to the transformation strain.

5.4. Strain evolution

5.4.1. Austenite strains in monolithic NiTi. In Fig. 10, if data from NiTi (S1) are considered alone (as reported previously [12]), the elastic lattice stain in the austenite in NiTi [from equation (2)] as a function of the applied compressive stress is mostly linear to 625 MPa. However, if a best fit line that includes data from both NiTi(S1) and NiTi(S2) is drawn (as in Fig. 10), the stress–strain response is linear to 450 MPa on loading but deviates slightly at higher stress. The slope of the deviation suggests that load is being transferred from austenite to martensite since progressively lesser strains are developed in the austenite. Furthermore, at a given stress on unloading, the strains obtained in austenite are larger in NiTi (S2) than NiTi (S1) (i.e. the diamond markers in Fig. 10 are consistently shifted to higher strains). From Figs 2 and 5, more martensite is present in NiTi (S1) than in NiTi (S2) at the same stress. If no load was being transferred from austenite to martensite, this difference in martensite volume fraction would have no effect and the austenite in both samples would ideally have the same strain response.

The observed behavior in Fig. 10 can be explained by taking into account the hysteresis in the macroscopic stress–strain curve in Fig. 2 and by assuming that load is indeed being transferred from austenite to martensite. The non-linearity in Fig. 10 can be assigned to: (i) different elastic constants between austenite and martensite, (ii) mismatch stresses between the two phases because of the transformation strains, and (iii) the evolving texture in the austenite (Section 5.3) and the consequent changes in elastic constants. As schematically sketched in Fig. 12(a), load transferred from austenite to martensite would result in the applied stress vs elastic strain response in austenite having a greater slope. As a result of the hysteresis, more martensite exists at the same stress during the unloading portion of the cycle as compared to the loading portion of the cycle (Fig. 2 and Ref. [11]). Thus, a greater portion of the applied stress remains transferred to the martensite down to lower applied stresses during the unloading part of the cycle and hence a shift in the austenite strain in NiTi (S2) is expected during unloading. A more realistic path based on the above proposed load transfer mechanism is shown as the dashed line in Fig. 10.

In the case of NiTi (S1), Fig. 10 indicates that there is little evidence of load transfer from austenite to martensite (unloading points are not shifted to larger strains). This is attributed to the lower volume fractions of martensite present and this preferentially-formed martensite being more compatible with the austenite since it comprises of favorable variants (with respect to stress and strain). The best fit line through the NiTi (S1) data has a slope of 74.5 GPa [12]. This apparent modulus compares well with the values obtained from the various averaging methods (72.9–75.4 GPa in Table 2). The best fit line through all the data (S1 and S2) has a slope of 71.5 GPa and also compares reasonably well. Agreement in the value of the apparent modulus (calculated using the applied stress) with the true modulus indicates that load transfer from austenite to martensite is minimal. Likewise, the data point corresponding to NiTi (S1) at 625 MPa shows very little deviation from a linear response in Fig. 10, even as 60% of austenite has transformed at this stress. At this point during the transformation, the strain mismatch between austenite and martensite is large, i.e. from Fig. 2, the overall macroscopic strain at 625 MPa is 2.8% while from Fig. 10, the measured elastic strain in austenite is only 0.9%. Thus, considering the magnitude of the deviation in Fig. 10, it can be concluded that the effects (i)–(iii) described previously that tend to cause non-linearity are either small or mostly cancel each other. The self-accommodating nature of the martensite results in certain variants preferentially forming to mostly minimize the mismatch with the transforming austenite.

5.4.2. Austenite and TiC strains in NiTi–TiC. Figure 11 shows the elastic lattice strains in austenite and TiC for NiTi–TiC (S1) and (S2) as obtained by Rietveld refinement [equation (2)] and predicted from Eshelby theory. Owing to the mostly linear response of the unreinforced austenite (Fig. 10), values obtained from the single-crystal averaging methods for austenite (Table 2) were used to represent the matrix in the Eshelby predictions in Fig. 11. The same elastic constants listed earlier were used for TiC.

The mismatch between the martensite, the transforming austenite and the TiC can be expected to be:

(a) elastic, i.e. due to the difference in elastic constants;

(b) thermal, i.e. due to the difference in coefficients of thermal expansion; and

(c) allotropic, i.e. due to the transformation strains (e.g. from Fig. 2, at maximum load the composite shows an overall macroscopic strain of 3% while from Fig. 11, the measured elastic lattice strain is 1% in austenite and 0.4% in TiC).

Despite the magnitude of the allotropic mismatch, Fig. 11 shows reasonable agreement between Eshelby theory (which accounts for only the elastic and thermal mismatches) and the individual phase strains measured by neutron diffraction. This

suggests that the allotropic mismatch in (c) is effectively accommodated by the stress-induced martensite. Similar cancellation of the twinning mismatch was also observed in shape-memory NiTi–TiC composites deforming by martensite twinning [10].

The non-linearity in Fig. 11, suggests that there is some load that is transferred in austenite and TiC. The deviation from linearity is more pronounced in the case of NiTi–TiC (S2), which was loaded to 975 MPa. Consequently, the difference between the loading and unloading strains is larger in the case of NiTi–TiC (S2) than in NiTi–TiC (S1). This is similar to the case of the monolithic NiTi, where there is more load transferred when higher volume fractions of (and consequently less compatible) martensite exist. Using data from only NiTi–TiC (S1) gives a mostly linear response in excellent agreement with the Eshelby theory predictions as observed in Ref. [12]. The schematic in Fig. 12 outlines a possible load transfer mechanism taking the hysteresis into consideration while the dashed line in Fig. 11 shows a more realistic path. Consistent with the schematic in Fig. 12, Fig. 11 shows lower strains in TiC during unloading for NiTi–TiC (S2). Again, data from both samples have been combined recognizing that the effect of temperature is negligible compared to the observed trends.

Owing to the duration of data acquisition at each stress level (approx. 6–8 h), data could only be obtained at a limited number of stress levels. This limitation together with the lack of quantitative strain information for the martensite precluded a quantitative statement on the load transfer mechanism.

5.4.3. Anisotropic components of strain. In Sections 5.4.1 and 5.4.2, the strains correspond to an average isotropic strain derived from equation (2). However, the Rietveld refinement procedure also incorporated anisotropic components of the strain [equation (3)]. The changes in slope in Fig. 13 suggest that the contribution of the anisotropic component to the total strain reverses direction. Consistent with our earlier observation and discussion for austenite in NiTi [17], this behavior cannot be explained by elastic anisotropy (i.e. anisotropy due to crystal geometry) but may be attributed to the additional anisotropy introduced by the transformation. The strain redistribution between grains as the austenite preferentially transforms to martensite is responsible for these changes. The strains at which the changes in anisotropy occur during the loading and unloading parts of the cycle are also indicated in Fig. 13 and a hysteresis is noted. The stresses corresponding to these strains are 370 MPa on loading and 290 MPa on unloading and compare well with the experimentally observed critical stresses for the onset and completion of the transformation in Fig. 2. The differences, if real, may be attributed to some initial anisotropy contribution from the transformation canceling the elastic contribution since they appear to act in opposite directions [17].

6. CONCLUSIONS

Rietveld refinement of neutron diffraction spectra has investigated stress-induced transformations in superelastic NiTi with and without 10 vol.% TiC particles. The following conclusions are reached.

1. The generalized spherical harmonic texture formulation in Rietveld refinement provides a determination of austenite and martensite phase fractions coexisting under an applied stress in NiTi and NiTi–TiC. A linear relationship is observed between the volume of stress-induced martensite and the macroscopic strain generated by the transformation for both NiTi and NiTi–TiC.
2. In NiTi and NiTi–TiC, the overall texture of the martensite decreases with increasing stress. This is attributed to favorable orientations of austenite transforming first to martensite and the need for the later-forming martensite to be compatible with the already transformed martensite (and TiC).
3. Significant discrepancies are observed between the Young's moduli for NiTi and NiTi–TiC measured by extensometry and predicted using single crystal data and Eshelby theory. The differences are attributed to small amounts of austenite transforming to martensite at low stresses which reduces the apparent moduli.
4. In contrast to the macroscopic data, the modulus of austenite in NiTi measured by neutron diffraction (from the slope of applied stress vs elastic strain response) compared well with moduli predicted using single crystal data (Hashin–Shtrikman bounds and Hill average).
5. The applied stress at which austenite transforms to martensite and back to austenite increases in the presence of TiC particles. The volume fraction of martensite formed at any given applied stress and the recoverable strain decrease in the presence of TiC particles.
6. For both NiTi and NiTi–TiC, the elastic lattice strain in the austenite remains linear with respect to the applied stress even when significant volume fractions of austenite have transformed to martensite, but shows some non-linearity at higher applied stress. This load transfer coupled with the stress hysteresis results in strains in the austenite during unloading being somewhat larger than strains during loading, for the same stress. For the composite, good agreement is observed in the phase strains predicted by Eshelby elastic theory and measured by neutron diffraction. In general, the self-accommodating nature of the stress-induced martensite almost

eliminates the mismatch with the TiC particles and the transforming austenite.

7. Additional anisotropy introduced by strain redistribution due to the transformation is reflected in changes in the anisotropic component of the strain of the austenite phase in NiTi–TiC.

Acknowledgements—The Manuel Lujan Jr Neutron Scattering Center is a national user facility funded by the US DOE, Office of Basic Energy Science and by Defense Programs. This work was supported in part by DOE Contract No. W-7405-ENG-36. R.V. and D.C.D. acknowledge the support of Daimler-Benz (Daimler-Chrysler) AG in the form of a research grant and R.V.'s participation in the MIT–Germany program.

REFERENCES

1. Duerig, T. W., Melton, K. N., Stoeckel, D. and Wayman, C. M., *Engineering Aspects of Shape Memory Alloys*. Butterworth-Heinemann, London, 1990.
2. Otsuka, K. and Wayman, C. M., *Shape Memory Materials*. Cambridge University Press, London, 1998.
3. Clyne, T. W. and Withers, P. J., *An Introduction to Metal Matrix Composites*. Cambridge University Press, London, 1993.
4. Mari, D. and Dunand, D. C., *Metall. Mater. Trans.*, 1995, **26A**, 2833.
5. Mari, D., Bataillard, L., Dunand, D. C. and Gotthardt, R., *J. Physique IV*, 1995, **5**, 659.
6. Fukami-Ushiro, K. L. and Dunand, D. C., *Metall. Mater. Trans.*, 1996, **27A**, 183.
7. Fukami-Ushiro, K. L., Mari, D. and Dunand, D. C., *Metall. Mater. Trans.*, 1996, **27A**, 193.
8. Dunand, D. C., Mari, D., Bourke, M. A. M. and Goldstone, J. A., *J. Physique IV*, 1995, **5**, 653.
9. Dunand, D. C., Mari, D., Bourke, M. A. M. and Roberts, J. A., *Metall. Mater. Trans.*, 1996, **27A**, 2820.
10. Dunand, D. C., Fukami-Ushiro, K. L., Mari, D., Roberts, J. A. and Bourke, M. A. M., in *Materials for Smart Systems II*, ed. E. P. George, R. Gotthardt, K. Otsuka, S. Trolier-McKinstry and M. Wun-Fogle. Materials Research Society, Pittsburg, PA, 1996, p. 131.
11. Bourke, M. A. M., Vaidyanathan, R. and Dunand, D. C., *Appl. Phys. Lett.*, 1996, **69**, 2477.
12. Vaidyanathan, R., Bourke, M. A. M. and Dunand, D. C., *Mater. Sci. Engng A*, in press.
13. Bourke, M. A. M., Goldstone, J. A. and Holden, T. M., in *Measurement of Residual and Applied Stress using Neutron Diffraction*, ed. M. T. Hutchings and A. D. Krawitz. Kluwer Academic, Dordrecht, 1992, p. 369.
14. Shi, N., Bourke, M. A. M., Roberts, J. A. and Allison, J. E., *Metall. Mater. Trans.*, 1997, **28A**, 2741.
15. Miyazaki, S., Imai, T., Igo, Y. and Otsuka, K., *Metall. Trans. A*, 1986, **17A**, 115.
16. Vaidyanathan, R., Ph.D. thesis, Massachusetts Institute of Technology, 1999.
17. Vaidyanathan, R., Bourke, M. A. M. and Dunand, D. C., *J. appl. Phys.*, in press.
18. Rietveld, H. M., *J. appl. Crystallogr.*, 1969, **2**, 65.
19. Larson, A. C. and Von Dreele, R. B., General Structure Analysis System (GSAS). Report No. LAUR 8-748, Los Alamos National Laboratory, 1986.
20. Bunge, H. J., *Texture Analysis in Materials Science*. Butterworth-Heinemann, London, 1982.
21. Von Dreele, R. B., *J. appl. Crystallogr.*, 1997, **30**, 517.
22. Daymond, M. R., Bourke, M. A. M. and Von Dreele, R. B., *J. appl. Phys.*, 1997, **82**, 1554.
23. Daymond, M. R., Bourke, M. A. M. and Von Dreele, R. B., *J. appl. Phys.*, 1999, **85**(2), 739.
24. Nye, J. F., *Physical Properties of Crystals*. Oxford Science, Oxford, 1985.
25. Plietsch, R. and Ehrlich, K., *Acta mater.*, 1997, **45**, 2417.
26. Leo, P. H., Shield, T. W. and Bruno, O. P., *Acta metall.*, 1993, **41**, 2477.
27. Miyazaki, S., Otsuka, K. and Suzuki, Y., *Scripta metall.*, 1981, **15**, 287.
28. McCormick, P. G. and Liu, Y., *Mater. Sci. Engng*, 1993, **A167**, 51.
29. Sturcken, E. F. and Croach, J. W., *Trans. metall. Soc. A.I.M.E.*, 1963, **227**, 934.
30. Raymond, M. R., Personal communication, 1997.
31. Poletika, T. M., Kulkov, S. N. and Panin, V. E., *Poroshkovaya Metallurgiya*, 1983, **7**(247), 54.
32. Kulkov, S. N., Poletika, T. M., Chukhlomin, A. Y. and Panin, V. E., *Poroshkovaya Metallurgiya*, 1984, **8**(260), 88.
33. Funakubo, H, *Shape Memory Alloys*. Gordon & Breach, London, 1987.
34. Johansen, K., Ph.D. thesis, Ruhr-Universität, 1998.
35. Salzbrenner, R. J. and Cohen, M., *Acta metall.*, 1979, **27**, 739.
36. Brill, T. M., Mittelbach, S., Assmus, W., Muellner, M. and Luethi, B., *J. Phys.: Condens. Matter*, 1991, **3**, 9621.
37. Mercier, O., Melton, K. N., Gremaud, G. and Haegi, J., *J. appl. Phys.*, 1980, **51**(3), 1833.
38. Hashin, Z. and Shtrikman, S., *J. Mech. Phys. Solids*, 1962, **10**, 335.
39. Voigt, W., *Lehrbuch der Krystallphysik*. Teubner, Leipzig, 1910.
40. Reuss, A., *Z. angew. Math. Mech.*, 1929, **9**, 49.
41. Hill, R., *Proc. Phys. Soc Lond.*, 1952, **A65**, 349.
42. Chang, R. and Graham, L. J., *J. appl. Phys.*, 1966, **37**, 3778.
43. Jackson, C. M., Wagner, H. J. and Wasilewski, R. J., 55-Nitinol—the alloy with a memory: its physical metallurgy, properties and applications. Report No. NASA-SP 5110, N72-30468 (NTISD), 1972.
44. Shackelford, J. and Alexander, W., *The CRC Materials Science and Engineering Book*. CRC Press, Boca Raton, FL, 1992.
45. Dunand, D. C. and Mortensen, A., *Mater. Sci. Engng A*, 1991, **135A**, 179.
46. Dunand, D. C. and Mortensen, A., *Acta metall. mater.*, 1991, **39**, 127.
47. Saburi, T. and Nenno, S., in *Solid–Solid Phase Transformations*, ed. H. I. Aaronson, D. E. Laughlin, R. F. Sekerka and C. M. Wayman. The Metallurgical Society of AIME, Warrendale, PA, 1981, p. 1455.
48. Olson, G. B. and Cohen, M., *Scripta metall.*, 1975, **9**, 1247.